Atmospheric Chemistry of Dimethyl Carbonate: Reaction with OH Radicals, UV Spectra of $CH_3OC(O)OCH_2$ and $CH_3OC(O)OCH_2O_2$ Radicals, Reactions of $CH_3OC(O)OCH_2O_2$ with NO and NO_2, and Fate of $CH_3OC(O)OCH_2O$ Radicals

M. Bilde, T. E. Møgelberg, J. Sehested,* and O. J. Nielsen*

Section for Chemical Reactivity, Environmental Science and Technology Department, Risø National Laboratory, DK-4000 Roskilde, Denmark

T. J. Wallington,* M. D. Hurley, S. M. Japar, and M. Dill

Research Staff, SRL-E3083, Ford Motor Company, P.O. Box 2053, Dearborn, Michigan 48121-2053

V. L. Orkin, T. J. Buckley, R. E. Huie, and M. J. Kurylo

Center for Chemical Physics, National Institute of Standards and Technology, Gaithersburg, Maryland 20899

Received: June 5, 1996; In Final Form: March 4, 1997[⊗]

A flash photolysis−resonance fluorescence technique was used to study the rate constant for the reaction of OH radicals with dimethyl carbonate over the temperature range 252−370 K. The rate constant exhibited a weak temperature dependence, increasing at both low and high temperature from a minimum value of approximately 3.1×10^{-13} cm^3 molecule^{-1} s^{-1} near room temperature. Pulse radiolysis/transient UV absorption techniques were used to study the ultraviolet absorption spectra and kinetics of $CH_3OC(O)OCH_2$ and $CH_3OC(O)CH_2O_2$ radicals at 296 K. Absorption cross sections of $CH_3OC(O)OCH_2$ and $CH_3OC(O)OCH_2O_2$ at 250 nm were $(3.16 \pm 0.34) \times 10^{-18}$ and $(3.04 \pm 0.43) \times 10^{-18}$ cm^2 molecule^{-1}, respectively. Rate constants measured for the self-reactions of $CH_3OC(O)OCH_2$ and $CH_3OC(O)OCH_2O_2$ radicals and reactions of $CH_3OC(O)OCH_2O_2$ radicals with NO and NO_2 were $(5.6 \pm 1.1) \times 10^{-11}$, $(1.27 \pm 0.21) \times 10^{-11}$, $(1.2 \pm 0.2) \times 10^{-11}$, and $(1.2 \pm 0.2) \times 10^{-11}$ cm^3 molecule^{-1} s^{-1}, respectively. The rate constant for reaction of F atoms with dimethyl carbonate was determined by a pulse radiolysis absolute rate technique to be $(6.1 \pm 0.9) \times 10^{-11}$ cm^3 molecule^{-1} s^{-1}. A FTIR smog chamber system was used to show that, in 760 Torr of air at 296 K, $CH_3OC(O)OCH_2O$ radicals are lost via three competing processes: 42 ± 15% via reaction with O_2, 14 ± 2% via H atom elimination, and 44 ± 10% via decomposition and/or isomerization. Relative rate techniques were used to measure rate constants for the reactions of F atoms with $CH_3OC(O)OCH_3$, $(6.4 \pm 1.4) \times 10^{-11}$ cm^3 molecule^{-1} s^{-1}, and Cl atoms with $CH_3OC(O)OCH_3$, $CH_3OC(O)OCH_2Cl$, $CH_3OC(O)OCHO$, and $HC(O)OC(O)OCHO$, $(2.3 \pm 0.8) \times 10^{-12}$, $(4.6 \pm 2.8) \times 10^{-13}$, $(1.7 \pm 0.1) \times 10^{-13}$, and $(1.7 \pm 0.1) \times 10^{-14}$ cm^3 molecule^{-1} s^{-1}, respectively. Results are discussed in the context of the atmospheric chemistry of $CH_3OC(O)OCH_3$.

1. Introduction

The use of oxygenated compounds in motor vehicle fuels is accelerating rapidly. In the United States this change in fuel composition has been pushed by the 1990 Clean Air Act Amendments. These amendments mandate the use of oxygenated fuels in areas of the United States which exceed the National Ambient Air Quality Standard for carbon monoxide during the winter and in the nine worst summer smog areas.

Under ideal conditions, oxygenated fuel components perform three simultaneous functions: to increase the fuel oxygen content (and thereby reduce CO emissions from carburated vehicles), to enhance the fuel octane value, and to lower the fuel's Reid vapor pressure (RVP). The currently preferred oxygenated fuel additives, ethanol and methyl *tert*-butyl ether (MTBE), have limitations. In particular, the use of ethanol effectively raises fuel RVP and, therefore, fuel-related evaporative emissions. For MTBE and other ethers such as ethyl *tert*-butyl ether (ETBE) and *tert*-amyl methyl ether (TAME), the relatively low oxygen content requires high blending volumes to meet fuel oxygen requirements. For example, to meet a 2.7 wt % O standard requires 15.1% (by volume) MTBE in a standard fuel.

Other oxygenated compounds, including organic carbonates,[1] have been suggested as potential oxygenated fuel additives because their use can minimize these problems. For example, dimethyl carbonate and diethyl carbonate have very high oxygen contents (53.3 and 40.6 wt %, respectively) compared to MTBE (18.2% wt oxygen), and their high boiling points can lead to a reduction in the RVP of the blended fuel.[1]

The potential use of organic carbonates in motor vehicle fuels introduces a general need to map out the oxidation mechanism of oxygenated organic molecules and necessitates an understanding of the environmental impact of such compounds if they are released into the atmosphere. This work addresses the oxidation mechanisms and atmospheric degradation of dimethyl carbonate (DMC).

Upon release to the atmosphere, DMC reacts with OH radicals:

$$CH_3OC(O)OCH_3 + OH \rightarrow CH_3OC(O)OCH_2 + H_2O \qquad (1)$$

As will be discussed, our measurements of k_1 are suggestive of both direct hydrogen abstraction as well as the formation of an addition complex that serves to facilitate such H atom abstraction. Thus, for atmospheric considerations, the products from reaction 1 can be considered as written. The oxygenated alkyl

[⊗] Abstract published in *Advance ACS Abstracts,* April 15, 1997.

S1089-5639(96)01664-7 CCC: $14.00

radical, $CH_3OC(O)OCH_2$, will then add oxygen within a few microseconds to form a peroxy radical:

$$CH_3OC(O)OCH_2 + O_2 + M \rightarrow CH_3OC(O)OCH_2O_2 + M \quad (2)$$

Peroxy radicals are removed from the atmosphere by reaction with NO, NO_2, HO_2, and other peroxy radicals ($R'O_2$).

$$CH_3OC(O)OCH_2O_2 + NO \rightarrow CH_3OC(O)OCH_2O + NO_2 \quad (3a)$$

$$CH_3OC(O)OCH_2O_2 + NO + M \rightarrow CH_3OC(O)OCH_2ONO_2 + M \quad (3b)$$

$$CH_3OC(O)OCH_2O_2 + NO_2 + M \rightarrow CH_3OC(O)OCH_2O_2NO_2 + M \quad (4)$$

$$CH_3OC(O)OCH_2O_2 + HO_2 \rightarrow \text{products} \quad (5)$$

$$CH_3OC(O)OCH_2O_2 + R'O_2 \rightarrow \text{products} \quad (6)$$

Neither the rate constants nor the products of reactions 1−6 have been determined experimentally. In this work the rate constants of reactions 1, 3, and 4 were investigated together with the UV absorption spectra of $CH_3OC(O)OCH_2$ and $CH_3OC(O)OCH_2O_2$ radicals. In addition, the atmospheric fate of the alkoxy radical, $CH_3OC(O)OCH_2O$, and the rate constants for the reactions of F and Cl atoms with DMC were determined.

2. Experimental Experimental

The three experimental systems used have been described previously.[2−6]

2.1. Flash Photolysis Resonance Fluorescence System. The flash photolysis resonance fluorescence (FPRF) technique was used to measure k_1. The principal apparatus component is a Pyrex reactor (of approximately 50 cm^3 internal volume) thermostated with a fluid circulated through its outer jacket. Reactions were studied in argon carrier gas (99.9995% purity supplied by Spectra Gases Inc.) at a total pressure of 100 Torr (0.75 Torr = 1 mbar = 2.46×10^{16} molecule cm^{-3}). Flows of dry argon, argon bubbled through water thermostated at 276 K, and DMC/argon mixtures were premixed and flowed through the reactor at a total flow rate between 0.69 and 1.4 cm^3 s^{-1}, STP. Different DMC/argon mixtures (0.5% and 1%) were used to verify that the dilution process did not introduce any systematic error into the rate constant measurement. Flow rates of both argon and H_2O/argon mixtures were measured by using calibrated Tylan mass flow meters, whereas that of DMC/argon mixture was determined by direct measurements of the rate of pressure change in the calibrated volume. The total pressure in the reactor was typically 100 Torr (as measured using an MKS Baratron manometer), with a water vapor component of approximately 0.07%. Hydroxyl radicals were produced by the pulsed photolysis (4 Hz repetition rate) of H_2O (introduced via the 276 K argon/H_2O bubbler) using a xenon flash lamp focused into the reactor. The OH radicals were then monitored by their resonance fluorescence near 308 nm excited by a microwave discharge resonance lamp (1.5 Torr of a 2% mixture of H_2O in UHP helium) focused into the reactor center. The resonance fluorescence signal was recorded on a computer-based multichannel scaler (time channel width 100 μs) as a summation of 3000−5000 consecutive flashes. The radical decay signal at each reactant concentration was analyzed as described by Orkin et al.[2] to obtain the first-order decay rate due to the reaction under study only (τ_{DMC}^{-1}). The sample of DMC used to obtain the k_1 values presented in Table 1 was a 99.9% purity liquid sample that was used with no further purificat after repeated freeze−pump−thaw cycles.

TABLE 1: Rate Constants[a] for the Reaction of OH with $(CH_3O)_2CO$

temp, K	no. of expt	[DMC] range, 10^{14} molecule cm^{-3}	$k_1 \times 10^{13}$, cm^3 $molecule^{-1}$ s^{-1}
252	4	0.53−2.83	3.33 ± 0.29
273	1	0.63−2.57	3.27 ± 0.13
277	5	0.53−2.56	3.14 ± 0.10
298	4	0.23−3.96	3.15 ± 0.07
330	3	0.42−3.68	3.32 ± 0.19
349	1	0.32−1.84	3.35 ± 0.13
370	4	0.35−2.47	3.82 ± 0.09

[a] Error bars are levels of confidence of 95% and do not include estimated systematic errors.

2.2. Pulse Radiolysis System. A pulse radiolysis transient UV absorption apparatus was used to study the UV absorption spectra and kinetics of $CH_3OC(O)OCH_2$ and $CH_3OC(O)OCH_2O_2$ radicals. Radicals were generated by radiolysis of gas mixtures in a 1 L stainless steel reactor by a 30 ns pulse of 2 MeV electrons from a Febetron 705B field emission accelerator. The radiolysis dose, referred to herein as a fraction of maximum dose, was varied by insertion of stainless steel attenuators between the accelerator and the chemical reactor. The analyzing light was obtained from a pulsed xenon arc lamp and reflected in the reaction cell by internal White type optics. The length of the cell is 10 cm; optical path lengths for the analysis light were 80 or 120 cm. The analyzing light was monitored by a 1 m McPherson monochromator linked to a Hamamatsu R928 photomultiplier and a LeCroy 9450A Oscilloscope. The monochromator was operated at a spectral resolution of 0.8 nm. UV absorption spectra were measured using a Princeton Applied Research OMA-II diode array installed at the exit slit of the monochromator in place of the photomultiplier. The monochromator was operated at a spectral resolution of 1.0 nm when used with the diode array. Spectral calibration was achieved using a Hg pen ray lamp. All transients were results of single pulse experiments with no signal averaging. Data acquisition, handling, and storage were performed by a standard PC computer. The uncertainties reported in this paper are two standard deviations unless otherwise stated. Standard error propagation methods are used to calculate combined uncertainties.

SF_6 was used as the diluent gas in the stainless steel reactor. Radiolysis of SF_6 produces fluorine atoms:

$$SF_6 + 2\ \text{MeV}\ e^- \rightarrow F + \text{products} \quad (7)$$

SF_6 was always present in great excess to minimize the relative importance of direct radiolysis of other compounds in the gas mixtures. The fluorine atom yield was determined by measuring the yield of CH_3O_2 radicals following radiolysis of mixtures of 10 mbar CH_4, 40 mbar O_2, and 950 mbar SF_6:

$$F + CH_4 \rightarrow CH_3 + HF \quad (8)$$

$$CH_3 + O_2 + M \rightarrow CH_3O_2 + M \quad (9)$$

CH_3O_2 radicals were monitored using their absorption at 260 nm. The absorbance at 260 nm is plotted as a function of radiolysis dose in the inset in Figure 1. At maximum dose, the absorbance falls below a linear extrapolation of the low dose data. This is ascribed to unwanted radical−radical reactions at high radical concentrations. A linear regression of the low dose

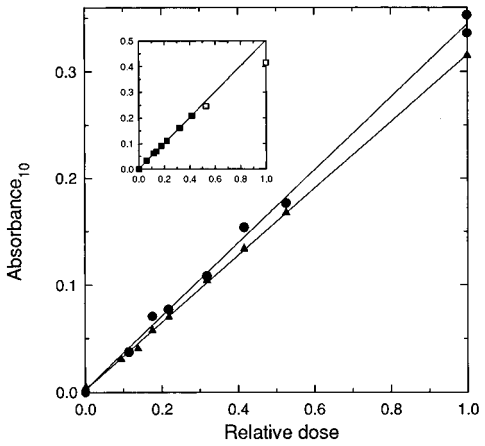

Figure 1. Maximum transient absorptions observed following radiolysis of mixtures of the following: 10 mbar of CH_4, 40 mbar of O_2, and 950 mbar of SF_6 (squares); 5 mbar of DMC, 40 mbar of O_2, and 955 mbar of SF_6 (triangles); and 20 mbar of DMC, and 980 mbar of SF_6 (circles). UV path lengths were 120, 80, and 80 cm, and the transients were recorded at 260, 250, and 250 nm, respectively. Solid lines are least-squares fit to the low dose data (filled symbols).

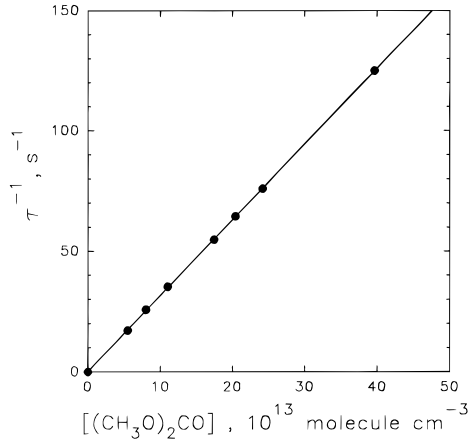

Figure 2. Plot of τ^{-1} versus [DMC] at $T = 298$ K for the reaction of OH with DMC. (The solid line is the linear least-square fit to the data).

data gives a slope of 0.50 ± 0.01, where the quoted error is 2 standard deviations. Combining this slope with $\sigma_{260nm}(CH_3O_2) = 3.18 \times 10^{-18}$ cm^2 molecule^{-1} [7] and the optical path length of 120 cm gives a F atom yield of $(3.18 \pm 0.32) \times 10^{15}$ cm^{-3} at full dose and 1000 mbar SF_6. The quoted uncertainty reflects both statistical uncertainty in the slope and a 10% uncertainty in $\sigma(CH_3O_2)$.[7]

Reagents used include the following: 20−40 mbar O_2 (ultra high purity); 950−1000 mbar SF_6 (99.9%); 0−20 mbar $CH_3OC(O)OCH_3$ (>99%); 0−0.2 mbar NO (>99.8%); 0−1.2 mbar NO_2 (>98%); and 0−10 mbar CH_4 (>99%). All were used as received. DMC was obtained at >99% purity and is a liquid at room temperature. The DMC sample was repeatedly degassed by freeze−pump−thaw cycles before use. $CH_3OC(O)OCH_2$ and $CH_3OC(O)OCH_2O_2$ radicals were generated by radiolysis of SF_6/DMC and SF_6/DMC/O_2 mixtures:

$$F + CH_3OC(O)OCH_3 \rightarrow CH_3OC(O)OCH_2 + HF \quad (10)$$

$$CH_3OC(O)OCH_2 + O_2 + M \rightarrow CH_3OC(O)OCH_2O_2 + M \quad (2)$$

2.3. FTIR-Smog Chamber System. The FTIR system was interfaced to a 140 L Pyrex reactor. Radicals were generated by the UV irradiation (22 blacklamps) of mixtures of 2.5−120 mTorr of DMC, 24−2000 mTorr of Cl_2, 0.1−700 Torr of O_2, and 0−37 mTorr of NO in 700 Torr total pressure with N_2 diluent at 296 K (760 Torr = 1013 mbar = 101 kPa). Loss of reactants and the formation of products were monitored by FTIR spectroscopy, using an analyzing path length of 27 m and a resolution of 0.25 cm^{-1}. Infrared spectra were derived from 32 coadded spectra. DMC, CO, $CH_3OC(O)OCHO$, HC(O)OC(O)OCHO, and CO_2 were monitored using their characteristic features over the wavenumber range 800−2500 cm^{-1}. Reference spectra of DMC, CO, and CO_2 were acquired and calibrated by expanding known volumes of reference materials into the reactor.

3. Results and Discussion

This section presents the oxidation mechanism of dimethyl carbonate. The order of the subsections follows the atmospheric degradation scheme of dimethyl carbonate.

First, the reaction of OH radicals with dimethyl carbonate was studied using the flash photolysis resonance fluorescence system. Second, the alkyl radical, $CH_3OC(O)OCH_2$, formed from reaction of DMC with OH, was studied using the pulsed radiolysis setup. In the pulsed radiolysis system the alkyl radicals were formed from the reaction of F atoms with DMC, and the UV absorption, formation, and decay kinetics of the $CH_3OC(O)OCH_2$ radicals were studied. In the atmosphere the alkyl radical reacts with O_2 to form $CH_3OC(O)OCH_2O_2$ radicals. The UV spectrum and self-reaction of the peroxy radical were studied using the pulsed radiolysis setup. In sections 3.5 and 3.6 the reactions of the $CH_3OC(O)OCH_2O_2$ radical with NO and NO_2 will be discussed. Before the atmospheric fate of the $CH_3OC(O)OCH_2O$ radical was studied, the reactions of dimethyl carbonate with F and Cl atoms were studied using the FTIR relative rate technique. The atmospheric fate of $CH_3OC(O)OCH_2O$ radicals was investigated using the FTIR system, and results are presented in section 3.9.

3.1. Kinetics of the Reaction of OH Radicals with Dimethyl Carbonate. Resonance fluorescence decays were treated as described in ref 2 to obtain first-order decay rates for each DMC concentration. A linear least-squares analysis of such first-order decays versus DMC concentration was used to determine a value for k_1 at each temperature. One such plot at 298 K is shown in Figure 2. Results from several analyses at each temperature were averaged to give the rate constants listed in Table 1, where the uncertainties expressed represent the 95% confidence intervals associated with the statistical analysis. (We estimate that total systematic errors associated with these measurements do not exceed an additional 5%.) The measured rate constants and their 95% confidence limits are plotted in Arrhenius form in Figure 3.

On the basis of both GC and GC−MS analyses a sample purity was ca. 99.9% with methanol (ca. 0.1%) as a main impurity. An original sample contained also CO_2 (ca. 0.02%) and three other impurities at levels of less than 0.01%, 0.002%, 0.001%, respectively, which we have not identified. The rate constant for the reaction of OH with CH_3OH is such (7.7×10^{-13} cm^3 molecule^{-1} s^{-1} at $T = 277$ K[8]) that this reaction can contribute far less than 1% to the measured value of k_1. The levels of other impurities are too low to influence the measured rate constant value, even if they react at collision rate. Therefore, an original sample of DMC has been only degassed before dilution with argon for measurements. In addition to concerns about any possible influence of reactive impurities, secondary chemistry must also be considered as a source of systematic errors. OH can react with both the radical products of the reaction under study as well as with relatively stable

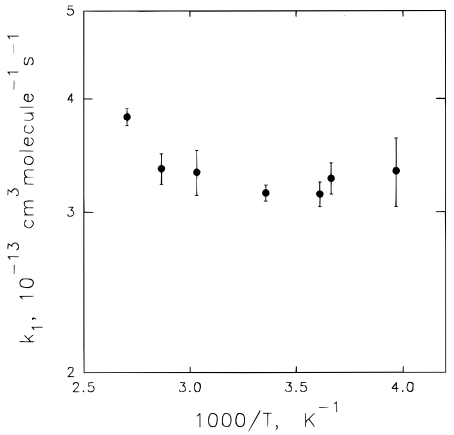

Figure 3. Arrhenius plot of the measured k_1 values with their 95% confidence intervals.

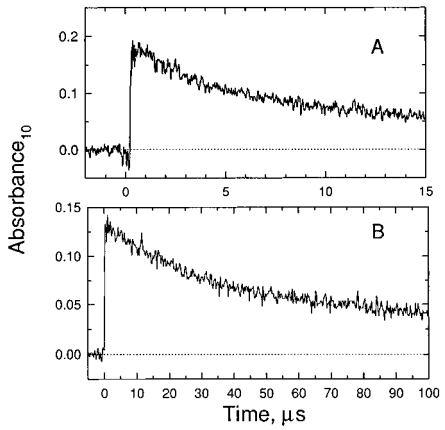

Figure 4. Transient absorption following radiolysis of mixtures of (A) 20 mbar DMC, and 980 mbar of SF_6, dose 52 of maximum, optical path length 80 cm; (B) 5 mbar of DMC, 40 mbar of O_2, and 955 mbar of SF_6, dose 42% of maximum, optical path length 80 cm. Both were recorded at 250 nm. Absorption is ascribed to (A) $CH_3OC(O)OCH_2$ radicals and (B) $CH_3OC(O)OCH_2O_2$ radicals.

products that can accumulate in the reactor because of the multiflash experimental procedure. As a check on these possibilities, several different experiments were performed. These experiments included varying the OH concentration by more than a factor of 5 via changes in either the flash energy or the water vapor concentration, reductions in the flow rate by more than a factor of 2, and reduction in total pressure by a factor of 5. In each case, the derived rate constants were statistically indistinguishable from those derived under the typical conditions described earlier.

There are no other studies of reaction 1 with which we can compare the present results. Nevertheless several observations can be made. First, the rate constant obtained for DMC is nearly 1 order of magnitude slower than that for the reaction of OH with dimethyl ether[9] but slightly greater than that for the similar reaction with acetone[10] and nearly identical to that for methyl acetate.[11] Thus it appears that the carbonyl function in DMC, acetone and methyl acetate exerts a strong negative influence on the reactivity of neighboring CH_3 groups. Secondly, the unusual temperature dependence of the rate constant merits comment. Despite the very small variation of the rate constant over the complete temperature range, these changes lie outside of the statistical uncertainty of the individual points. Thus, there appears to be a slight increase in the rate constant as the temperature is either raised or lowered about room temperature. This behavior is in contrast with that for acetone[10] but is nearly identical with that observed for methyl acetate.[11] As discussed in earlier studies of OH reactivity with oxygenated organics,[10,11] we believe that the temperature behavior is indicative of two pathways for hydrogen abstraction. At higher temperatures direct hydrogen abstraction dominates and, as in the case of acetone, is associated with normal Arrhenius behavior. An increase in rate constant with decreasing temperature is associated with the formation of an addition complex (such as depicted below) that is stabilized by decreasing temperature and facilitates abstraction from a CH_x group located β to the carbonyl group. Such a β group is present in DMC and methyl acetate, thereby allowing formation a six-membered cyclic intermediate, but not in acetone. At higher temperatures, the adduct is less stable and the direct pathway for hydrogen abstraction dominates.

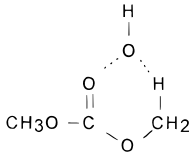

3.2. UV Absorption, Formation, and Decay Kinetics of the $CH_3OC(O)OCH_2$ Radical. UV absorption, formation, and decay kinetics of a large number of alkyl radicals have been studied in our laboratory using the pulsed radiolysis setup. See refs 6, 12, and 13 for details and examples. Figure 4A shows the transient absorbance observed at 250 nm upon radiolysis of a mixture of 20 mbar of DMC and 980 mbar of SF_6. To determine the absorption cross section of the $CH_3OC(O)OCH_2$ radical at 250 nm the maximum transient absorbance was measured at various doses. Figure 1 (circles) shows a plot of the absorbance as a function of the dose. The absorbance is proportional to the dose up to full dose which shows that radical−radical reactions such as 11 and 12 at high initial radical concentrations are not of significant importance.

$$CH_3OC(O)OCH_2 + CH_3OC(O)OCH_2 + M \rightarrow \text{products} \quad (11)$$

$$CH_3OC(O)OCH_2 + F \rightarrow \text{products} \quad (12)$$

The absorption cross section of the $CH_3OC(O)OCH_2$ radical was determined from the slope of a linear regression of the dose data in Figure 1, 0.342 ± 0.014, the fluorine atom yield, $(3.18 \pm 0.32) \times 10^{15}$ molecules cm^{-3} at full dose and 1000 mbar of SF_6, and the optical path length, 80 cm. The absorption cross section of $CH_3OC(O)OCH_2$ radicals at 250 nm calculated from these three values is $(3.16 \pm 0.34) \times 10^{-18}$ cm^2 molecule^{-1}. The UV absorption spectrum was acquired using the diode array with a radiolysis dose which was 42% of the maximum and an optical path length of 80 cm. The spectrum was recorded 0.5 μs after the electron pulse, the gate time was 5 μs, and the resolution was 0.96 nm. Absorption cross sections of $CH_3OC(O)OCH_2$ in the interval 240−340 nm were then determined by scaling the absorbance at 250 nm to the absorption cross section derived above. The result is shown in Figure 5. Selected absorption cross sections obtained as averages of five data points are given in Table 2.

The rate constant for the self-reaction of $CH_3OC(O)OCH_2$ radicals was determined by monitoring the decay rate of the absorption at 250 nm. The half-lives of the decays were derived from a fit of a second-order decay mechanism to the data: $A(t) = A_{inf} + (A_0 - A_{inf})/(1 + 2k'(A_0 - A_{inf})t)$, where $A(t)$ is the time dependent absorbance, A_0 and A_{inf} are the absorbances at $t = 0$, and at $t = \infty$, respectively, and $k' = k_{11}\sigma_{CH_3OC(O)OCH_2}(250\text{ nm}) \times l/2.303$. The decays were always well fit by the

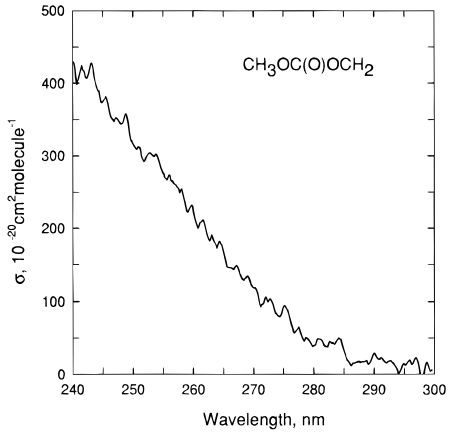

Figure 5. Spectrum of the $CH_3OC(O)OCH_2$ radical.

TABLE 2: Measured UV Absorption Cross Sections

wavelength, nm	$\sigma(CH_3OC(O)OCH_2)$ $\times 10^{20}$, cm^2 molecule^{-1}	$\sigma(CH_3OC(O)OCH_2O_2)$ $\times 10^{20}$, cm^2 molecule^{-1}
240	428	427
250	316	304
260	225	192
270	119	106
280	40	58
290	27	34
300	8	17

second-order expression above. In Figure 6 the reciprocal of the decay half-lives at various doses, derived from the decay transients at 250 nm, are plotted against the maximum transient absorbance. From a linear regression analysis of the data a slope of $(1.02 \pm 0.07) \times 10^5$ s^{-1} was established. This slope equals $k_{11}(2 \times 2.303)/(l\sigma_{CH_3OC(O)OCH_2}(250\text{ nm}))$ where k_{11} is the rate constant for reaction 11, l is the optical path length, 80 cm, and $\sigma_{CH_3OC(O)OCH_2}(250\text{ nm}) = (3.16 \pm 0.34) \times 10^{-18}$ cm^2 molecule^{-1}. Hence, $k_{11} = (5.6 \pm 0.7) \times 10^{-11}$ cm^3 molecule^{-1} s^{-1}. We estimate that potential systematic errors could add an additional 10% to the uncertainty range, and we choose to quote an uncertainty of 20%. Propagating this uncertainty gives $k_{11} = (5.6 \pm 1.1) \times 10^{-11}$ cm^3 molecule^{-1} s^{-1}.

The absorption of $CH_3OC(O)OCH_2$ radicals at 230 nm was used to determine k_{10}. A first-order formation expression was fitted to the rise of the observed transients at 230 nm immediately after the radiolysis pulse for various initial concentrations of $CH_3OC(O)OCH_3$ (0.51−3.01 mbar). The expression used was $A(t) = (A_{inf} - A_0)(1 - \exp(-k^{1st}t)) + A_0$, where $A(t)$ is the time dependent absorbance, A_{inf} is the absorbance at infinite time, and A_0 is the extrapolated absorbance at time $t = 0$. Values of k^{1st} obtained are plotted as a function of the $CH_3OC(O)OCH_3$ concentration in Figure 7. A linear least-squares fit gives $k_{10} = (6.1 \pm 0.6) \times 10^{-11}$ cm^3 molecule^{-1} s^{-1}. This is in good agreement with the $(6.4 \pm 1.4) \times 10^{-11}$ cm^3 molecule^{-1} s^{-1} determined using a relative rate technique described in section 3.7. There is a small positive intercept in Figure 7 of $(4.1 \pm 2.7) \times 10^5$ s^{-1}. The likely reason for this intercept is a contribution to radical loss by secondary reactions such as 11 and 12. Secondary chemistry causes a determination of k_6 that is too high because the maximum absorbance is reached too early. Therefore secondary chemistry such as reactions 11 and 12 give a positive intercept. To investigate this possibility, simulations of the absorbance transients for $[DMC]_0 = 0.51$ and 2.51 mbar were performed using a chemical mechanism consisting of reactions 10 and 11 with $k_{10} = k_{11} = 6 \times 10^{-11}$ cm^3 molecule^{-1} s^{-1} and $\sigma_{CH_3OC(O)OCH_2} = (4.81 \pm 0.53) \times 10^{-11}$ cm^2 molecule^{-1}. The numerical integrations were performed using the CHEMSIMUL numerical integration program.[14] The simulated transients were then fitted using the same expression used for the experimental data. The pseudo-first-order formation rates obtained were 1.0×10^6 s^{-1} for $[DMC]_0 = 0.51$ mbar and 4.3×10^6 s^{-1} for $[DMC]_0 = 2.51$ mbar. These two points are shown as hollow circles in Figure 7. As seen in the figure there is excellent agreement between the simulated points and the experimental data. We conclude that the small positive intercept in Figure 7 is caused by loss of $CH_3OC(O)OCH_2$ radicals via reaction 11 and that the value of k_{10} derived above needs no significant correction. We estimate that potential systematic errors could add an additional 10% to the uncertainty range. Propagating this additional uncertainty gives $k_{10} = (6.1 \pm 0.9) \times 10^{-11}$ cm^3 molecule^{-1} s^{-1}.

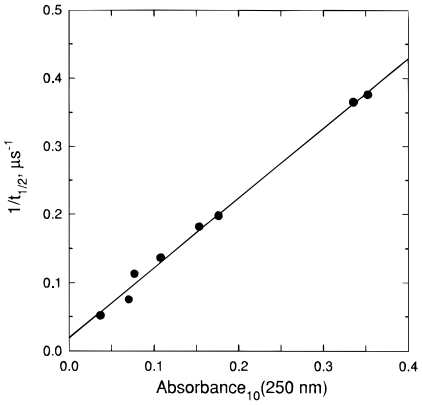

Figure 6. The reciprocal half-lives for the self-reaction of $CH_3OC(O)OCH_2$ radicals (monitored at 250 nm) versus the maximum transient absorbance. The solid line is a linear regression.

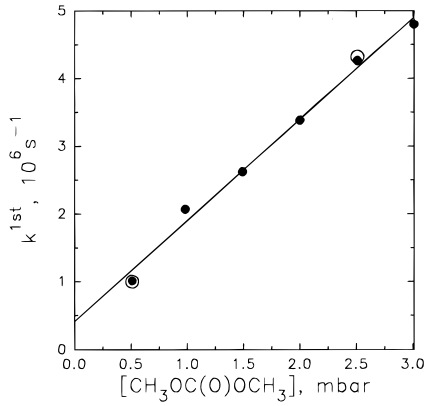

Figure 7. First-order rate constants for the reaction of F atoms with DMC obtained from fits to the observed increase in absorption at 230 nm following pulse radiolysis of mixtures of 0.51−3.01 mbar of DMC and 1000 mbar of SF_6 versus the initial DMC concentration. Hollow circles show the results from computer simulations.

3.3. UV Absorption Spectrum of the $CH_3OC(O)OCH_2O_2$ Radical. UV absorption spectra and kinetics of the self-reaction of a large number of peroxy radicals have been studied in our chamber, and results and methods have recently been described.[15,16] The chemistry of peroxy radicals has been reviewed in refs 17 and 19.

When mixtures of 5 mbar of DMC, 40 mbar of O_2, and 955 mbar of SF_6 were subject to pulse radiolysis, a transient absorbance was observed between 220 and 300 nm. Varying $[O_2]$ by a factor of 1.5 and [DMC] by a factor of 5 had no discernible effect on the observed transient absorbance (dose = 0.42, UV path length = 80 cm). An example of an experimental absorption transient at 250 nm is shown in Figure 4B. We attribute this absorption to the formation of $CH_3OC(O)OCH_2O_2$ radicals by the consecutive set of reactions 7, 10, and 2.

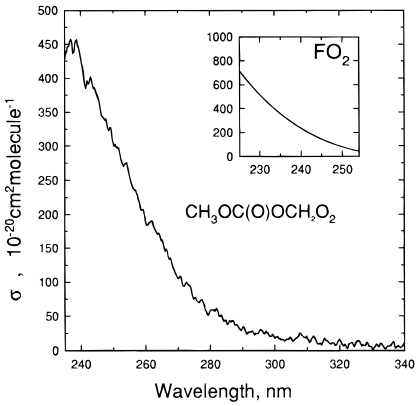

Figure 8. Spectrum of the $CH_3OC(O)OCH_2O_2$ radical.

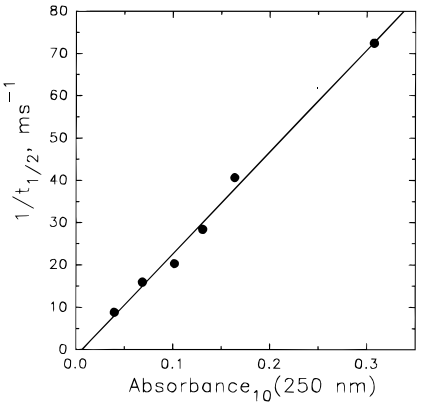

Figure 9. The reciprocal half-lives of the decay of $CH_3OC(O)OCH_2O_2$ radicals due to self-reaction (monitored at 250 nm) versus the maximum transient absorbance. The solid line is obtained by linear regression to the experimental data.

To quantify the UV absorption spectrum of the $CH_3OC(O)OCH_2O_2$ radical, its concentration needs to be determined. The yield of the $CH_3OC(O)OCH_2O_2$ radicals can only be obtained if a known fraction of the F atoms are converted into $CH_3OC(O)OCH_2O_2$ radicals. Unwanted secondary radical-radical reactions such as reactions 6 and 11−14 must be avoided or minimized.

$$CH_3OC(O)OCH_2O_2 + CH_3OC(O)OCH_2O_2 \rightarrow \text{products} \quad (6)$$

$$CH_3OC(O)OCH_2 + CH_3OC(O)OCH_2 + M \rightarrow \text{products} \quad (11)$$

$$CH_3OC(O)OCH_2 + F \rightarrow \text{products} \quad (12)$$

$$CH_3OC(O)OCH_2O_2 + CH_3OC(O)OCH_2 \rightarrow \text{products} \quad (13)$$

$$CH_3OC(O)OCH_2O_2 + F \rightarrow \text{products} \quad (14)$$

In addition, the reaction of F atoms with O_2 needs to be minimized:

$$F + O_2 + M \rightarrow FO_2 + M \quad (15)$$

To minimize the amount of F atoms consumed by reaction 15 the oxygen concentration should be low. However, a low oxygen concentration will increase the importance of reactions 11−13. Clearly a compromise is needed. An initial O_2 concentration of 40 mbar was chosen. Under these experimental conditions, 2.4% of the F atoms are converted into FO_2 ($k_{15} = 1.9 \times 10^{-13}$ (ref 18) and $k_{10} = 6.1 \times 10^{-11}$ cm^3 molecule^{-1} s^{-1}). Absolute values for the absorption cross sections (in units of 10^{-20} cm^2 molecule^{-1}) of FO_2 at different wavelengths are[18] $\sigma_{225nm} = 755$, $\sigma_{230nm} = 508$, $\sigma_{235nm} = 341$, $\sigma_{240nm} = 180$, $\sigma_{245nm} = 153$, $\sigma_{254nm} = 69$ and can be used to correct for the absorbance due to this radical. A "continuous" spectrum of FO_2 in the interval 225−254 nm was obtained from a fifth order fit to these data and is shown in the inset in Figure 8.

There are no literature data concerning the kinetics of reactions 12−14; hence we cannot calculate their importance. To check for these unwanted radical−radical reactions, the transient absorption at 250 nm was measured in experiments using $[CH_3OC(O)OCH_3] = 5$ mbar, $[O_2] = 40$ mbar, and $[SF_6] = 955$ mbar with the radiolysis dose varied over 1 order of magnitude. The UV path length was 80 cm. Figure 1 (triangles) shows the observed maximum of the transient absorption as a function of the dose. As seen from Figure 1, the absorption is linear with radiolysis dose indicating that secondary reactions are not important. The solid line drawn through the data in Figure 1 is a linear least-squares fit to the data which gives a slope of 0.314 ± 0.005. From this and three additional pieces of information, (i) the F atom yield of (3.18 ± 0.32) × 10^{15} cm^{-3} (full dose and $[SF_6] = 1000$ mbar), (ii) the conversion of F atoms into 97.6% $CH_3OC(O)OCH_2O_2$ and 2.4% FO_2, and (iii) the absorption cross section for FO_2 at 250 nm ($\sigma = 1.26 \times 10^{-18}$ cm^2 molecule^{-1} [19]), we derive $\sigma(CH_3OC(O)OCH_2O_2)$ at 250 nm = (3.04 ± 0.31) × 10^{-18} cm^2 molecule^{-1}. The quoted error is two standard deviations from the linear least-squares fit to all the data indicated by triangles in Figure 1. In addition, we need to account for uncertainty in the absolute calibration of the fluorine atom yield. Propagating this uncertainty, we arrive at $\sigma_{CH_3OC(O)OCH_2O_2}(250\text{ nm}) = (3.04 \pm 0.43) \times 10^{-18}$ cm^2 molecule^{-1}.

To map out the spectrum of the $CH_3OC(O)OCH_2O_2$ radical, experiments were performed using the diode array with a radiolysis dose of 0.42 and an optical path length of 80 cm. The spectrum was recorded 5 μs after the electron pulse, with a gate time of 5 μs. The spectrum was placed on an absolute basis by scaling to $\sigma(250\text{ nm}) = 3.04 \times 10^{-18}$ cm^2 molecule^{-1}. A small correction (<8.5%) was applied to correct for the formation of FO_2 using the formula: $\sigma_{corrected} = (\sigma_{raw} - \sigma_{FO_2}\text{-}(0.024))/0.976$. The result is shown in Figure 8, and selected absorption cross sections are listed in Table 2.

3.4. Self-Reaction of the $CH_3OC(O)OCH_2O_2$ Radical. Figure 4B shows a typical transient absorption obtained following the pulsed radiolysis of DMC/SF_6/O_2 mixtures. The decay of the absorption transient is due to the self-reaction of the $CH_3OC(O)OCH_2O_2$ radical:

$$CH_3OC(O)OCH_2O_2 + CH_3OC(O)OCH_2O_2 \rightarrow \text{products} \quad (6)$$

The rate constant of reaction 6 is defined by the equation $-d[CH_3OC(O)OCH_2O_2]/dt = 2k_6[CH_3OC(O)OCH_2O_2]^2$. The observed rate constant k_{6obs} for reaction 6 can be derived from a plot of the reciprocal half-lives of the peroxy radical decay versus the maximum transient absorbance measured at 250 nm. Figure 9 shows such a plot. The absorbances are corrected for the absorption due to FO_2 according to the formula $A = A_{obs} - \sigma(FO_2) \times 80$ cm × 0.024 × 3.02 × 10^{15} molecule cm^{-3} × dose. The decay half-lives were derived from a fit to the data using the second-order expression: $A(t) = A_{inf} + (A_0 - A_{inf})/(1 + 2k(A_0 - A_{inf})t)$, where $A(t)$ is the time dependent absorbance, A_0, and A_{inf} are the absorbances at $t = 0$, and at $t = \infty$, respectively. $k = k_6 l \sigma_{CH_3OC(O)OCH_2O_2}(250\text{ nm})/2.303$ where k_6 is the second-order rate constant for the self-reaction of the radicals. The decays were always well described by second-order kinetics. For these experiments the optical path length

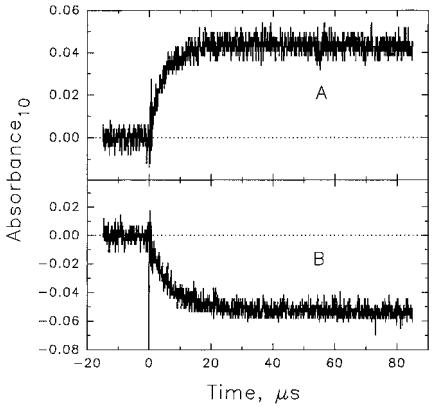

Figure 10. Transient absorption at 400 nm due to NO_2 following radiolysis (53% of maximum dose) of mixtures of the following: (A) 0.46 mbar of NO, 5 mbar of DMC, 20 mbar of O_2 and 975 mbar of SF_6; (B) 0.57 mbar of NO_2, 5 mbar of DMC, 20 mbar of O_2 and 975 mbar of SF_6.

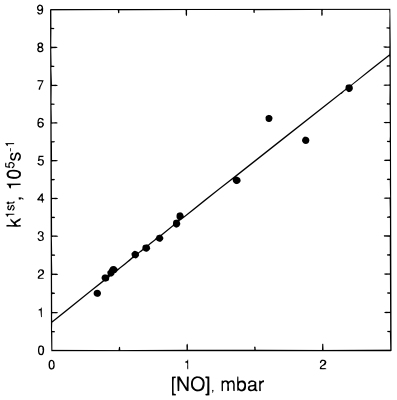

Figure 11. First-order formation rates of NO_2 (formed from the reaction of NO with $CH_3OC(O)OCH_2O_2$) observed following radiolysis of SF_6/DMC/O_2/NO mixtures as a function of NO concentration.

was 80 cm, [DMC] = 5 mbar, [O_2] = 40 mbar, [SF_6] = 955 mbar, and the dose was varied between full and 14%.

A linear regression analysis of the data in Figure 9 gives a slope of $(2.41 \pm 0.20) \times 10^5$ s^{-1}. This slope equals $k_{6obs}(2 \times 2.303)/(l\sigma_{CH_3OC(O)OCH_2O_2}(250\ nm))$ where k_{6obs} is the observed rate constant for reaction 6, l is the optical path length, 80 cm, and $\sigma_{CH_3OC(O)OCH_2O_2}(250\ nm) = (3.04 \pm 0.43) \times 10^{-18}$ cm^2 molecule^{-1}. Hence, $k_{6obs} = (1.27 \pm 0.21) \times 10^{-11}$ cm^3 molecule^{-1} s^{-1}. In addition to reaction 6, the decay of the $CH_3OC(O)OCH_2O_2$ radical may also be influenced by reactions with other radicals, for example:

$$CH_3OC(O)OCH_2O + O_2 \rightarrow HO_2 + CH_3OC(O)OCHO \quad (16)$$

$$HO_2 + CH_3OC(O)OCH_2O_2 \rightarrow \text{products} \quad (17)$$

$$CH_3OC(O)OCH_2O_2 + CH_3OC(O)OCH_2O \rightarrow \text{products} \quad (18)$$

Since the rate constants for reactions 16−18 are unknown, we cannot correct for these reactions at the present time. It is, however, interesting to compare the reaction of HO_2 with a series of other peroxy radicals, i.e. CH_3O_2, $CH_3CH_2O_2$, $HOCH_2O_2$, and $CH_3C(O)O_2$. The rate constants for the self-reactions are 5.8×10^{-12}, 5.8×10^{-12}, 1.2×10^{-11}, and 1.4×10^{-11} cm^3 molecule^{-1} s^{-1}, respectively.[19] The rate is seen to increase significantly with the introduction of an alcohol or carbonyl group into the molecule. It is also of interest to compare the rate constants for the self-reaction of different peroxy radicals. Consider the series CH_3O_2, $CH_3CH_2O_2$, $HOCH_2O_2$, $CH_3OCH_2O_2$, $CH_3C(O)CH_2O_2$, and $CH_3OC(O)OCH_2O_2$. The rate constants for the self-reactions are 3.7×10^{-13}, 6.6×10^{-14}, 6.2×10^{-12}, 2.7×10^{-12}, 8.3×10^{-12},[19] and 1.27×10^{-11} (observed only) [this work], respectively. The rate is seen to increase with the introduction of oxygen into the molecule.

3.5. Rate Constant for the Reaction between $CH_3OC(O)OCH_2O_2$ and NO. The rate constant for the reaction of NO with $CH_3OC(O)OCH_2O_2$ was studied using the pulsed radiolysis setup. Following the radiolysis of SF_6/DMC/O_2/NO mixtures an increase in absorption at 400 nm was observed. Figure 10A shows a typical absorption transient. The experiments were performed using half dose (full dose produces 3.2×10^{15} F atoms), with mixtures of 5 mbar of DMC, 20 mbar of O_2, 975 mbar of SF_6, and 0.34−2.20 mbar of NO. The increase in absorption is ascribed to NO_2 formation via reaction 3a. For each concentration of NO the increase in absorption was fitted using the following expression for a first-order formation: $A(t) = (A_{inf} - A_0)(1 - \exp(-k^{1st}t)) + A_0$, where $A(t)$ is the time dependent absorbance, A_0 is the extrapolated absorbance at time $t = 0$, A_{inf} is the absorbance at infinite time, and k^{1st} is the pseudo-first-order appearance rate of NO_2. This technique for measuring the rate constant for the reaction of NO with peroxy radicals has most recently been described in ref 15. To allow time for the conversion of F atoms to $CH_3OC(O)OCH_2O_2$ radicals, the transients were fitted from time $t = 2$ μs. The rate constant k_3 for the decay of $CH_3OC(O)OCH_2O_2$ due to reaction with NO was determined from the slope of a plot of pseudo-first-order rate constants versus concentration of NO. The plot is seen in Figure 11. The slope gives $k_{3obs} = (1.2 \pm 0.1) \times 10^{-11}$ cm^3 molecule^{-1} s^{-1}. The y-axis intercept is $(7 \pm 2) \times 10^4$ s^{-1} and suggests that radical reactions such as the self-reaction of the $CH_3OC(O)OCH_2O_2$ radicals may contribute to the loss of $CH_3OC(O)OCH_2O_2$ radicals. The yield of NO_2 was calculated using $\sigma(NO_2) = 6.02 \times 10^{-19}$ cm^2 molecule^{-1} at 400 nm[8] and was in the range 55−85%. This is consistent with secondary loss of RO_2 radicals. We choose to add an additional 15% to the uncertainty range of k_{3obs}. Propagating this additional uncertainty gives an observed rate constant for the reaction of NO with $CH_3OC(O)OCH_2O_2$ of $k_{3obs} = (1.2 \pm 0.2) \times 10^{-11}$ cm^3 molecule^{-1} s^{-1}.

3.6. Rate Constant for the Reaction between $CH_3OC(O)OCH_2O_2$ and NO_2. To study reaction 4, the NO_2 decay at 400 nm was observed following the radiolysis of NO_2/DMC/O_2/SF_6 mixtures. A series of experiments was performed varying the NO_2 concentration between 0.28−1.19 mbar. The radiolysis dose was 52% of maximum. Figure 10B shows a typical absorption transient. For each experiment the absorption transient was fitted using a first-order decay, and a pseudo-first-order rate constant was determined. The fits were made from 3 μs to allow time for the formation of the $CH_3OC(O)OCH_2O_2$ radical. The fitted first-order decay rates of NO_2 are plotted in Figure 12 as a function of NO_2 concentration together with a linear regression of the experimental data. The slope gives $k_4 = (1.2 \pm 0.1) \times 10^{-11}$ cm^3 molecule^{-1} s^{-1}. We estimate that potential systematic errors could add an additional 10% to the uncertainty range. Propagating this additional uncertainty gives $k_4 = (1.2 \pm 0.2) \times 10^{-11}$ cm^3 molecule^{-1} s^{-1}.

3.7. Relative Rate Studies of the Reactions of Cl and F Atoms with $CH_3OC(O)OCH_3$. Prior to investigating the atmospheric fate of $CH_3OC(O)OCH_2O$ radicals, relative rate experiments were performed using the FTIR system to investigate the kinetics of reactions 10 and 20. The techniques used are described in detail elsewhere.[20] Photolysis of molecular

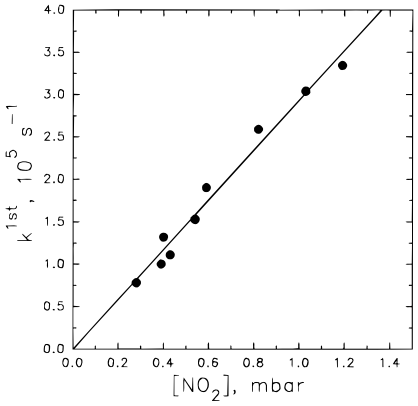

Figure 12. First-order rates of NO_2 loss (monitored at 400 nm) due to reaction of NO_2 with $CH_3OC(O)OCH_2O_2$ plotted versus NO_2 concentration.

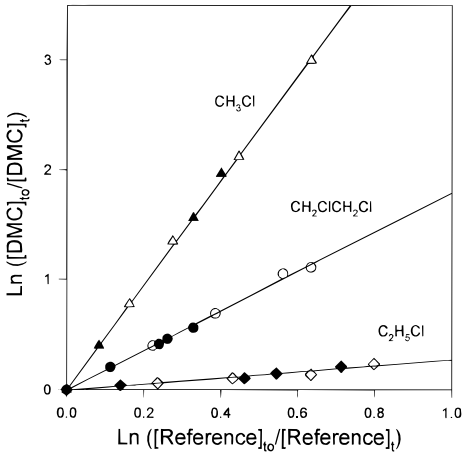

Figure 13. Decay of DMC versus CH_3Cl (triangles), CH_2ClCH_2Cl (circles), and C_2H_5Cl (diamonds) in the presence of Cl atoms in 700 Torr of air (filled symbols) or N_2 (open symbols).

halogen was used as a source of halogen atoms.

$$Cl_2 \text{ (or } F_2) + h\nu \rightarrow 2Cl \text{ (or } 2F) \quad (19)$$

$$Cl + CH_3OC(O)OCH_3 \rightarrow CH_3OC(O)OCH_2 + HCl \quad (20)$$

$$F + CH_3OC(O)OCH_3 \rightarrow CH_3OC(O)OCH_2 + HF \quad (10)$$

The kinetics of reaction 20 were measured relative to reactions 22−24. Reaction 10 was measured relative to reactions 25 and 26.

$$Cl + C_2H_5Cl \rightarrow \text{products} \quad (22)$$

$$Cl + CH_3Cl \rightarrow \text{products} \quad (23)$$

$$Cl + CH_2ClCH_2Cl \rightarrow \text{products} \quad (24)$$

$$F + CH_4 \rightarrow CH_3 + HF \quad (25)$$

$$F + CD_4 \rightarrow CD_3 + DF \quad (26)$$

The observed losses of $CH_3OC(O)OCH_3$ versus those of reference compounds in the presence of either Cl or F atoms are shown in Figures 13 and 14, respectively. There was no discernible difference between data obtained in 700 Torr of either N_2 or air diluent. Linear least-squares analysis gives $k_{20}/k_{22} = 0.28 \pm 0.07$, $k_{20}/k_{23} = 4.74 \pm 0.15$, $k_{20}/k_{24} = 1.79 \pm 0.10$, $k_{10}/k_{25} = 0.92 \pm 0.05$, and $k_{10}/k_{26} = 1.39 \pm 0.06$. Using

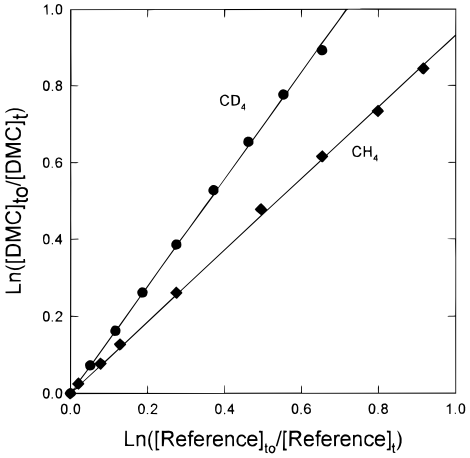

Figure 14. Decay of DMC versus CD_4 (circles) and CH_4 (diamonds) in the presence of F atoms in 700 Torr of air.

$k_{22} = 8.04 \times 10^{-12}$,[21] $k_{23} = 4.9 \times 10^{-13}$,[8] $k_{24} = 1.3 \times 10^{-12}$,[22] $k_{25} = 6.8 \times 10^{-11}$,[23] and $k_{26} = 4.7 \times 10^{-11}$ [23] gives $k_{20} = (2.3 \pm 0.6) \times 10^{-12}$, $k_{20} = (2.3 \pm 0.1) \times 10^{-12}$, $k_{20} = (2.3 \pm 0.1) \times 10^{-12}$, $k_{10} = (6.3 \pm 0.3) \times 10^{-11}$, and $k_{10} = (6.5 \pm 0.3) \times 10^{-11}$ cm^3 molecule^{-1} s^{-1}, respectively. We estimate that potential systematic errors associated with uncertainties in the reference rate constants could add an additional 10% and 20% uncertainty ranges for k_{20} and k_{10}, respectively. Propagating these additional uncertainties gives values of $k_{20} = (2.3 \pm 0.8) \times 10^{-12}$, $k_{20} = (2.3 \pm 0.2) \times 10^{-12}$, $k_{20} = (2.3 \pm 0.2) \times 10^{-12}$, $k_{10} = (6.3 \pm 1.3) \times 10^{-11}$, and $k_{10} = (6.5 \pm 1.3) \times 10^{-11}$ cm^3 molecule^{-1} s^{-1}. We choose to cite final values of k_{20} and k_{10} which are averages of those determined using the two different reference compounds together with error limits which encompass the extremes of the two individual determinations. Hence, $k_{20} = (2.3 \pm 0.8) \times 10^{-12}$ and $k_{10} = (6.4 \pm 1.4) \times 10^{-11}$ cm^3 molecule^{-1} s^{-1}. Quoted error reflects the accuracy of our measurements. The value of k_{10} determined using the FTIR technique is in agreement with the determination of $k_{10} = (6.1 \pm 0.6) \times 10^{-11}$ cm^3 molecule^{-1} s^{-1} using the pulse radiolysis technique (see section 3.2). There are no literature data available for k_{20} or k_{10} with which to compare our results.

3.8. Study of the Relative Reactivity of $CH_3OC(O)OCH_2$ Radicals toward Cl_2 and O_2. The rate constant ratio k_{27}/k_2 was measured using the FTIR-Smog chamber system at Ford Motor Co. by irradiating DMC/Cl_2/O_2/N_2 mixtures with UV light and observing the dependence of the yield of the chloride, $CH_3OC(O)OCH_2Cl$, on the [Cl_2]/[O_2] concentration ratio.

$$CH_3OC(O)OCH_2 + Cl_2 \rightarrow CH_3OC(O)OCH_2Cl + Cl \quad (27)$$

The first task in this set of experiments was to obtain a calibrated spectrum of the chloride which is unavailable commercially. To obtain a reference spectrum for this compound, mixtures of 5.2 mTorr of DMC and 0.1−2.0 Torr of Cl_2 in 700 Torr of N_2 diluent were irradiated. In the absence of O_2, and for sufficiently small conversions of DMC, it is expected that reactions 20 and 27 will convert DMC quantitatively into $CH_3OC(O)OCH_2Cl$. Following the irradiation of DMC/Cl_2/O_2/N_2 mixtures, IR product features were observed. For consumptions of DMC of 5−75%, these product features increased linearly with the loss of DMC, and it seems reasonable to ascribe these features to $CH_3OC(O)OCH_2Cl$. The spectrum of $CH_3OC(O)OCH_2Cl$ obtained is shown in Figure 15B together with a reference spectrum of DMC (15A). The IR features of DMC at 996, 1272, 1454, and 1788 cm^{-1} have been assigned to H_3C-O stretching, OCO asymmetric stretching, CH_3 symmetric deformation, and

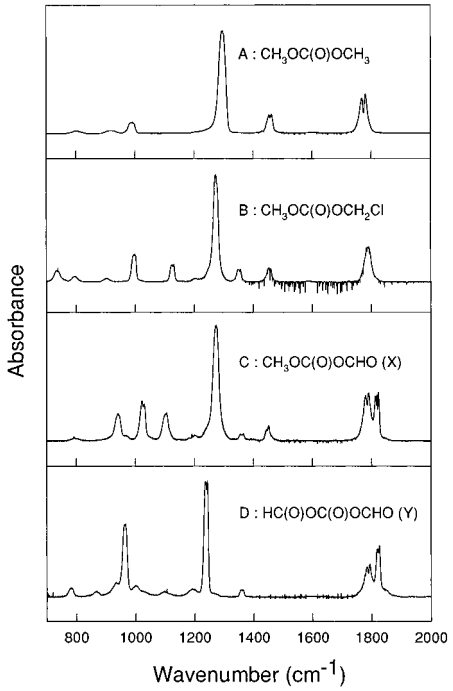

Figure 15. IR spectra of the following: (A) DMC, $\sigma(1296\ cm^{-1}) = 4.1 \times 10^{-18}$; (B) $CH_3OC(O)OCH_2Cl$, $\sigma(1272\ cm^{-1}) = 3.7 \times 10^{-18}$; (C), $CH_3OC(O)OCHO$, $\sigma(1271\ cm^{-1}) = 4.9 \times 10^{-18}$; (D) $HC(O)OC(O)OCHO$, $\sigma(1238\ cm^{-1}) = 5.9 \times 10^{-18}\ cm^2\ molecule^{-1}$.

C═O stretching modes, respectively.[24] As a result of the loss of symmetry, the IR spectrum of $CH_3OC(O)OCH_2Cl$ is more complex than that of DMC. The IR feature at 734 cm^{-1} in the chloride spectrum is typical for a C−Cl stretch mode.[25]

Following irradiation of DMC/Cl_2/N_2 mixtures the concentration of $CH_3OC(O)OCH_2Cl$ increased linearly with DMC loss until 70−80% of the DMC was consumed. With further irradiation the concentration of $CH_3OC(O)CH_2Cl$ leveled off and then decreased, presumably reflecting reaction with Cl atoms. By modeling the dependence of the $CH_3OC(O)OCH_2Cl$ yield on the fractional DMC loss, we were able to establish that Cl atoms react with $CH_3OC(O)OCH_2Cl$ at a rate which is 0.2 ± 0.1 times that of reaction 20. Thus, $k(Cl + CH_3OC(O)OCH_2Cl) = (4.6 \pm 2.8) \times 10^{-13}\ cm^3\ molecule^{-1}\ s^{-1}$.

Addition of O_2 to the reaction mixtures suppressed the chloride yield. This behavior is expected as the added O_2 competes with reaction 27 for the available $CH_3OC(O)OCH_2$ radicals. Experiments were performed at a constant total pressure of 700 Torr (N_2 diluent) with the concentration ratio $[Cl_2]/[O_2]$ varied over the range 0.07−0.80. As discussed elsewhere,[26] a plot of $Y_{Cl}/(1 - Y_{Cl})$ versus $[Cl_2]/[O_2]$, where Y_{Cl} is the molar chloride yield, $\Delta[CH_3OC(O)OCH_2Cl]/\Delta[CH_3OC(O)OCH_3]$, should be linear passing through the origin with a slope of k_{27}/k_2. Figure 16 shows such a plot. Linear least-squares analysis of the data in Figure 16 gives $k_{27}/k_2 = 2.2 \pm 0.2$. For completeness, a series of experiments were performed to study the effect of total pressure on k_{27}/k_2. Experiments were conducted at 10, 20, 50, and 100 Torr total pressure, and the results gave values of $k_{27}/k_2 = 1.9 \pm 0.2$, 1.8 ± 0.2, 2.0 ± 0.2, and 1.8 ± 0.2, respectively. There was no discernible effect of total pressure over the range 10−700 Torr, suggesting reaction 2 is at, or near, the high-pressure limit over this pressure range. Such behavior is reasonable considering the kinetic data base for alkyl radicals of this size.[27] The fraction of alkyl radicals $CH_3OC(O)OCH_2$ that reacts with O_2 is given by $1/(1 + 2.2[Cl_2]/[O_2])$. In section 3.9 experimental conditions were chosen to ensure that all (>97%) of the alkyl radicals react with

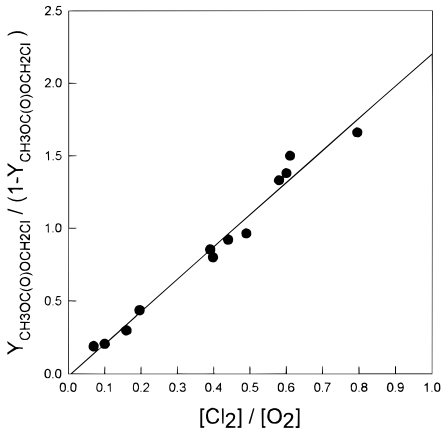

Figure 16. Plot of $Y_{CH_3OC(O)OCH2Cl}/(1 - Y_{CH_3OC(O)OCH_2Cl})$ versus $[Cl_2]/[O_2]$ for experiments conducted at 700 Torr total pressure and 295 ± 2 K.

O_2 and not Cl_2. Where appropriate, small corrections were applied to account for chloride formation.

3.9. Study of the Atmospheric Fate of $CH_3OC(O)OCH_2O$ Radicals. The results from the pulse radiolysis study show that the peroxy radical derived from DMC reacts rapidly with NO to give NO_2 and, by implication, $CH_3OC(O)OCH_2O$ radicals. The fate of $CH_3OC(O)OCH_2O$ radicals is expected to be either C−O bond scission, H atom elimination, reaction with O_2, or a combination of these processes.

$$CH_3OC(O)OCH_2O + M \rightarrow CH_3OC(O)O + HCHO + M \quad (28)$$

$$CH_3OC(O)OCH_2O + M \rightarrow CH_3OC(O)OCHO + H + M \quad (29)$$

$$CH_3OC(O)OCH_2O + O_2 \rightarrow CH_3OC(O)OCHO + HO_2 \quad (30)$$

To investigate the atmospheric fate of $CH_3OC(O)OCH_2O$ radicals, experiments were conducted using the FTIR-Smog chamber system in which DMC/Cl_2/O_2 mixtures, with and without added NO, were subject to UV irradiation. In these experiments the alkoxy radical $CH_3OC(O)OCH_2O$ was produced either via the peroxy radical self-reaction 31 or via reaction 3a.

$$2CH_3OC(O)OCH_2O_2 \rightarrow 2CH_3OC(O)OCH_2O + O_2 \quad (31)$$

The aim of the FTIR experiments was to establish the relative importance of reactions 28−30 under atmospheric conditions. HCHO is produced in reaction 28. However, because Cl atoms react 32 (7.3×10^{-11} [8]/2.3×10^{-12}) times faster with HCHO than with DMC, for experiments employing measurable consumptions of DMC (>2%), any HCHO product formed will react substantially with Cl atoms to give CO. Thus, in place of HCHO, CO serves as a marker for reaction 28. The $CH_3OC(O)O$ radical formed in reaction 28 is a stable species at 295 K,[28] and it is not obvious how this radical will react in the system. By analogy to methyl formate which is formed during the oxidation of dimethyl ether,[29] $CH_3OC(O)OCHO$ formed in reactions 29 and 30 is expected to be a stable and relatively unreactive compound in the chamber.

In the first experiment a mixture of 5.33 mTorr of DMC and 94.7 mTorr of Cl_2 in 700 Torr of O_2 diluent was subjected to a series of successive 20−60 s UV irradiations. In these experiments the IR features attributable to DMC decreased and were replaced by IR features of an unknown product(s) at 940, 1024, 1101, 1271, 1358, 1451, 1784, and 1817 cm^{-1}. Further irradiation of the sample led to increases of the IR features of

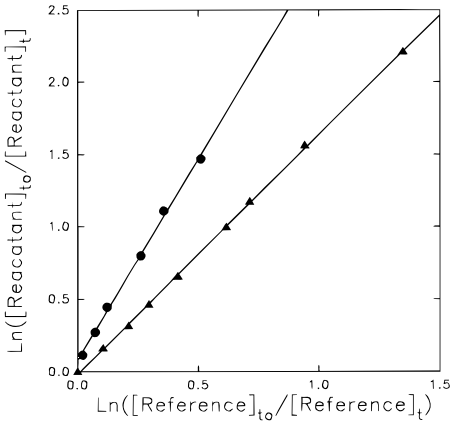

Figure 17. Decay of $CH_3OC(O)OCHO$ versus CH_4 (▲) and HC(O)OC(O)CHO versus CD_4 (●) in the presence of Cl atoms in 700 Torr of O_2.

the unknown(s) until the consumption of the DMC was almost complete (>90% loss). Continued irradiation led to little or no increase in X until all the DMC had been consumed (>98%) at which point the concentration of X started to decrease. The IR features scaled linearly during both formation and loss in the chamber, suggesting (but not proving) that they are all attributable to a single chemical species which we will designate "X". To test for reactions occurring in the absence of UV light reaction, mixtures were allowed to stand in the dark for 10 min between irradiations; there was no observable change in the IR spectra showing the absence of complications associated with "dark chemistry". The fact that little, or no, loss of X was observed until almost all of the DMC had been consumed shows that its reactivity toward Cl atoms is substantially less than that of DMC. Further irradiation led to a decrease in X and the formation of a new set of unknown IR features at 961, 1238, 1788, and 1822 cm^{-1}. This second set of IR product features increased at the expense of X upon further irradiation. Only when >90% of X was consumed did the second set of unknown features decrease. The IR features of the second unknown scaled linearly during both formation and loss in the chamber, again suggesting (but not proving) that they are all attributable to a single chemical species which we will designate "Y". Y is much less reactive toward Cl atoms than X. The spectra of the unknowns X and Y are given in Figure 15C,D. We believe these spectra can be assigned to $CH_3OC(O)OCHO$ and HC(O)OC(O)OCHO, respectively. While this "assignment" is based largely upon the kinetic and mechanistic evidence that is presented below, it is supported by the gross features of the IR spectra in Figure 15C,D. Thus, both spectra show two carbonyl stretching features at 1750−1850 cm^{-1}, with the feature at lower frequency similar to that in DMC (panel 15A) presumably attributable to the central C═O group. When compared to this feature, the second carbonyl feature, which is attributed to the C═O at the end of the molecule, is approximately twice as intense in panel 15D than in 15C consistent with the presence of two terminal C═O groups. As expected from the increased symmetry, the spectrum in panel 15D is simpler than for 15C. The IR feature at 1457 cm^{-1} in DMC (see 15A) is caused by symmetric deformation of the CH_3 group.[24] Consistent with expectations, a similar feature is present in panel 15C but absent in 15D.

Kinetic data for the reactivity of Cl atoms with $CH_3OC(O)OCHO$ and HC(O)OC(O)OCHO were obtained in two separate experiments. Both experiments started with a mixture of 5 mTorr of DMC and 200 mTorr of Cl_2 in 700 Torr of O_2 diluent. In the first experiment the mixture was subject to successive 10 s UV irradiations until the DMC was completely consumed. CH_4 was then added, and the irradiations were continued with the loss of CH_4 and $CH_3OC(O)OCHO$ monitored. In the second experiment the DMC/Cl_2/O_2 mixture was irradiated until both the DMC and $CH_3OC(O)OCHO$ were completely consumed. CD_4 was then added, and the irradiations were continued with the loss of CD_4 and HC(O)OC(O)OCHO monitored. Figure 17 show plots of the loss of $CH_3OC(O)OCHO$ versus CH_4 and the loss of HC(O)OC(O)OCHO versus CD_4. Linear least-squares analysis gives $k_{32}/k_{33} = 1.7 \pm 0.1$ and $k_{34}/k_{35} = 2.8 \pm 0.2$.

$$Cl + CH_3OC(O)OCHO \rightarrow \text{products} \quad (32)$$

$$Cl + CH_4 \rightarrow HCl + CH_3 \quad (33)$$

$$Cl + HC(O)OC(O)OCHO \rightarrow \text{products} \quad (34)$$

$$Cl + CD_4 \rightarrow DCl + CD_3 \quad (35)$$

Using $k_{33} = 1.0 \times 10^{-13}$ [8] and $k_{35} = 6.1 \times 10^{-15}$ [20] gives $k_{32} = (1.7 \pm 0.1) \times 10^{-13}$ and $k_{34} = (1.7 \pm 0.1) \times 10^{-14}$ cm^3 $molecule^{-1}$ s^{-1}. It is interesting to note the strong deactivating effect that replacing the CH_3 group by a HC(O) group has in these molecules. Moving from $CH_3OC(O)OCH_3$ to $CH_3OC(O)OCHO$ to HC(O)OC(O)OCHO the reactivity toward Cl atoms decreases by factors of 14 and 10, respectively. Such behavior is similar to that displayed by the structurally similar molecules CH_3OCH_3 and CH_3OCHO in which a decrease in reactivity toward Cl atoms by a factor of 136 (1.9×10^{-10} [30]/1.4×10^{-12} [31]) is observed.

In experiments using DMC/Cl_2 mixtures in 700 Torr of O_2 diluent, there was little evidence of CO formation as DMC was converted into $CH_3OC(O)OCHO$. The CO yield, expressed as moles of CO formed per mole of DMC lost, was ∼10%. In light of the relative unreactivity of Cl atoms toward DMC and the small yield of CO, we cannot exclude the possibility that a substantial fraction, if not all, of the observed CO is attributable to reaction of Cl atoms with small amounts of reactive impurities in the chamber such as HCHO which may be present in the chamber. Reaction 28 is clearly of minor importance in 700 Torr of O_2 diluent. Reactions 29−30 lead to the formation of HO_2 radicals which could react with the peroxy radicals from DMC and complicate the mechanistic analysis. To investigate this possibility, experiments were performed using DMC/Cl_2/NO/O_2/N_2 mixtures. The NO in these experiments served two purposes. First, it reacted rapidly with the peroxy radicals formed from DMC, converting them into alkoxy radicals and thereby avoiding any unwanted products from the peroxy radical self-reaction. Second, it scavenged HO_2 radicals, converting them into OH radicals and thereby avoiding hydroperoxide formation. In the first experiment, the initial conditions were as follows: 5.18 mTorr of DMC, 91.5 mTorr of Cl_2, 18.4 mTorr of NO, and 650 Torr of O_2 in 700 Torr total pressure with N_2 diluent. These conditions were chosen to be as close as possible to those employed in the absence of NO. Following a series of 1 min UV irradiations the DMC was observed to decay and IR features attributable to $CH_3OC(O)OCHO$ appeared linearly with DMC loss. With the exception of a small yield (∼20%) of CO, no other carbon-containing products were observed, suggesting that channel 3b is of negligible importance. The $CH_3OC(O)OCHO$ yield in experiments with, and without, NO was indistinguishable within the experimental uncertainties (10%). The behavior of DMC is similar to that observed in experiments using dimethyl ether. Cl atom initiated oxidation of CH_3OCH_3 with, and without, NO produces methyl formate (CH_3OCHO) as the dominant product.[29,32]

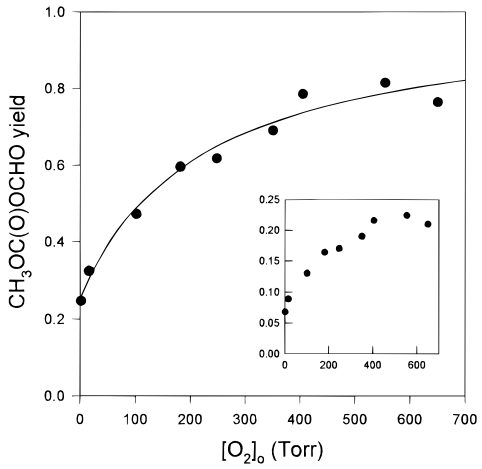

Figure 18. Yield of $CH_3OC(O)OCHO$ following the UV irradiation of $DMC/Cl_2/NO/O_2/N_2$ mixtures as a function of the O_2 partial pressure at constant total pressure (700 Torr) and 295 ± 2 K.

Next, experiments were performed to investigate the effect of O_2 partial pressure on the $CH_3OC(O)OCHO$ yield using mixtures of 5.1−5.5 mTorr of DMC, 24−94 mTorr of Cl_2, 9.7−30 mTorr of NO, and 1.9−650 Torr of O_2 in 700 Torr total pressure with N_2 diluent. Variation of the NO concentration from 6 to 20 mTorr at the lowest O_2 partial pressure of 1.9 Torr with all other parameters held fixed had no discernible effect on the $CH_3OC(O)OCHO$ yield. The results are presented as the inset in Figure 18, which shows that the $CH_3OC(O)OCHO$ yield (displayed in arbitrary units in the insert) decreased as the O_2 partial pressure was lowered. However, even in the presence of only 1.9 Torr of O_2, formation of $CH_3OC(O)OCHO$ was appreciable. Such behavior suggests that reactions 29 and 30 both contribute to $CH_3OC(O)OCHO$ formation.

As the $[O_2]$ partial pressure was decreased, the yield of CO increased. At the lowest $[O_2]$ pressure the molar yield of CO (moles of CO formed per mole of DMC consumed) was 150%. In addition, an unidentified product(s) with IR features at 986, 1190, and 1274 cm^{-1} was observed. At this point it should be stressed that because of the absence of an authentic sample of $CH_3OC(O)OCHO$, the yields plotted in the inset are in arbitrary units. Assuming that reaction 3 proceeds entirely via channel 3a and that $CH_3OC(O)OCH_2O$ radicals are lost via reactions 28−30, the $CH_3OC(O)OCHO$ yield is

$$Y(CH_3OC(O)OCHO) = \left(\frac{\left(\frac{k_{30}}{k_{29}}\right)[O_2] + 1}{\left(\frac{k_{30}}{k_{29}}\right)[O_2] + 1 + \left(\frac{k_{28}}{k_{29}}\right)} \right)$$

This expression was fitted to the data in the inset in Figure 18 with three parameters varied simultaneously: k_{30}/k_{29}, k_{28}/k_{29}, and a linear scaling factor (used to convert the arbitrary units in the insert into absolute units in Figure 18). Best fit values of $k_{30}/k_{29} = 0.018 \pm 0.006$ $Torr^{-1}$ and $k_{28}/k_{29} = 3.0 \pm 0.6$ were obtained. Using these results it can be calculated that in the presence of 1 atm of air diluent ($[O_2] = 160$ Torr) reactions 28−30 account for 44 ± 10%, 14 ± 2%, and 42 ± 15% of the fate of $CH_3OC(O)OCH_2O$ radicals.

Thus far we have neglected the possible isomerization of the alkoxy radical via internal H atom abstraction which could proceed through a 7-membered ring transition state. It has been shown by Eberhard et al.[33] and Atkinson and Aschmann[34] that such processes are important for aliphatic C_6 and C_7 alkoxy radicals. Isomerization may also play a role in the fate of $CH_3OC(O)OCH_2O$ radicals. The analysis presented above is unaffected if reaction 28 is replaced, or augmented, by isomerization.

Finally, we need to consider how these results fit in with the available data concerning the atmospheric degradation mechanisms of other alkoxy radicals. The results from the present work show that under atmospheric conditions at least three (possibly four, if isomerization is also important) loss mechanisms compete for $CH_3OC(O)OCH_2O$ radicals. A similar conclusion was reached in a recent study of the alkoxy radical derived from dimethoxymethane, $CH_3OCH_2OCH_2O$.[35] There are obvious structural similarities between this alkoxy radical and that derived from DMC, so similar behavior is not unexpected.

Veyret et al. and Jenkin et al. have presented evidence for H atom elimination from $HOCH_2O$ and CH_3OCH_2O radicals, with rates at 298 K of $k_{36} \approx 1200$ s^{-1} [36] and $k_{37} \approx 3000$ s^{-1}.[32]

$$HOCH_2O + M \rightarrow HCOOH + H + M \qquad (36)$$

$$CH_3OCH_2O + M \rightarrow CH_3OCHO + H + M \qquad (37)$$

From $k_{30}/k_{29} = 0.018$ $Torr^{-1}$ and assuming $k_{30} \approx 10^{-14}$ cm^3 $molecule^{-1}$ s^{-1} (typical for such a type of reaction 27), an estimate of $k_{29} = 2 \times 10^4$ s^{-1} is obtained which is broadly comparable to the rates of the analogous reactions 36 and 37. It appears that H atom elimination may be a general decomposition mechanism for alkoxy radicals bearing an oxygen functionality.

4. Conclusions

A substantial body of kinetic and mechanistic data pertaining to the atmospheric chemistry of dimethyl carbonate is presented here. It is shown that DMC reacts slowly with OH radicals. At 277 K, OH radicals react with dimethyl carbonate 46 ($3.1 \times 10^{-13}/6.7 \times 10^{-15}$ [8]) times faster than with methyl chloroform. Methyl chloroform has an atmospheric lifetime of 5.7 years with respect to reaction with OH radicals;[37,38] hence, the atmospheric lifetime of dimethyl carbonate is approximately 2 months. To provide information on the likely importance of photolysis of DMC, we searched for UV absorption at 250, 275, 300, and 350 nm. No significant absorption was observed. At 350 nm an upper limit of $\sigma < 5 \times 10^{-22}$ cm^2 $molecule^{-1}$ was derived. In light of the absence of detectable absorption and by analogy to the behavior of structurally similar compounds such as esters[39] it is unlikely that photolysis of DMC is of any atmospheric importance. Reaction with OH gives an alkyl radical which is converted rapidly into the corresponding peroxy radical. Using $k_3 = 1.2 \times 10^{-11}$ cm^3 $molecule^{-1}$ s^{-1} together with an estimated background tropospheric NO concentration of 2.5×10^8 cm^{-3},[40] the lifetime of the peroxy radical with respect to reaction 3 is 6 min. Reaction 3 is likely to be an important atmospheric loss of the peroxy radical. It is shown here that reaction 3 produces NO_2 and (by inference) alkoxy radicals.

In 1 atm of air diluent at 296 K, 56% of the alkoxy radicals are converted into $CH_3OC(O)OCHO$ which, by analogy to its behavior toward Cl atoms, is expected to be relatively unreactive to further OH radical attack. The remaining 44% of the alkoxy radicals either decompose via C−O bond scission or undergo isomerization via a 1,7 H atom shift. The reactivity of DMC toward OH radicals is low and is comparable to that of ethane. When compared to conventional fuels, the ozone-forming potential of DMC will be negligible. While a full assessment requires measurement of emissions from DMC-fueled vehicles, the present work suggests that, from the viewpoint of ozone

formation, use of DMC in automobile fuels would not be environmentally harmful.

From the viewpoint of understanding the atmospheric degradation mechanism of organic compounds, it is interesting to note that the alkoxy radical derived from DMC undergoes three competing atmospheric loss processes. This is a very unusual case as typically only one, or perhaps two, processes are important. Evidence is presented showing rapid H atom elimination from the alkoxy radical derived from DMC. This may be a general decomposition mechanism for alkoxy radicals bearing an oxygen functionality.

Acknowledgment. We thank Roscoe Carter (Ford) for helpful discussions regarding the IR spectra in Figure 15.

References and Notes

(1) Battacharya, A. K.; Boulanger, E. M. Preprints, Division of Environmental Chemistry, Meeting of the American Chemical Society, Washington, D.C., 1994, p 471.

(2) Orkin, V. L.; Huie, R. E.; Kurylo, M. J. *J. Phys. Chem.* **1996**, *100*, 8907.

(3) Wallington, T. J.; Japar, S. M. *J. Atmos. Chem*. **1989**, *9*, 399.

(4) Hansen, K. B.; Wilbrandt, R.; Pagsberg, P. *Rev. Sci. Instr*. **1979**, *50*, 1532.

(5) Nielsen, O. J. Risø-R-480, Risø National Laboratory, Roskilde, Denmark, 1984.

(6) Sehested, J. Risø-R-804, Risø National Laboratory, Roskilde, Denmark, 1994.

(7) Wallington, T. J.; Dagaut, P.; Kurylo, M. J. *Chem. Rev*. **1992**, *92*, 667.

(8) DeMore, W. B.; Sander, S. P.; Golden, D. M.; Hampson, R. F.; Kurylo, M. J.; Howard, C. J.; Ravishankara, A. R.; Kolb, C. E.; Molina, M. J. Jet Propulsion Labotatory Publication 94-26, Pasadena, CA, 1994.

(9) Wallington, T. J.; Liu, R.; Dagaut, P.; Kurylo, M. J. *Int. J. Chem. Kinetics*. **1988**, *20*, 41.

(10) Wallington, T. J.; Kurylo, M. J. *J. Phys. Chem.* **1987**, *91*, 5050−54.

(11) Wallington, T. J.; Dagaut, P.; Liu, R.; Kurylo, M. J. *Int. J. Chem. Kinet.* **1988**, *20*, 177.

(12) Wallington, T. J.; Bilde, M.; Møgelberg, T. E.; Sehested, J.; Nielsen, O. J. *J. Phys. Chem*. **1996**, *100*, 5751.

(13) Wallington, T. J.; Ellermann, T.; Nielsen, O. J. *Res. Chem. Intermed.* **1994**, *20*, 265.

(14) Bjergbakke, E.; Sehested, K.; Rasmussen, O. L.; Christensen, H. Risø-M-2430, Risø National Laboratory, Roskilde, Denmark, 1984.

(15) Wallington, T. J.; Nielsen, O. J. *Progress and Problems in Atmospheric Chemistry, Advanced Series in Physical Chemistry*; World Scientific: River Edge,NJ, 1995; Vol. 3, p 616.

(16) Wallington, T. J.; Maricq, M. M.; Ellermann, T.; Nielsen, O. J. *J. Phys. Chem*. **1992**, 96, *982*.

(17) Wallington, T. J.; Dagaut, P.; Kurylo, M. J. *Chem. Rev*. **1992**, *92*, 667.

(18) Ellermann, T.; Sehested, J.; Nielsen, O. J.; Pagsberg, P.; Wallington, T. J. *Chem. Phys. Lett*. **1994**, *218*, 287.

(19) Lightfoot, P. D.; Cox, R. A.; Crowley, J. N.; Destriau, M.; Hayman, G. D.; Jenkin, M. E.; Moortgat, G. K.; Zabel, F. *Atmos. Environ*. **1992**, *26A*, 1805.

(20) Wallington, T. J.; Hurley, M. D. *Chem. Phys. Lett*. **1992**, *189*, 437.

(21) Wine, P. H.; Semmes, D. H. *J. Phys. Chem*. **1983**, *87*, 3572.

(22) Wallington, T. J.; Bilde, M.; Møgelberg, T. E.; Sehested, J.; Nielsen, O. J. *J. Phys. Chem.* **1996**, *100*, 5751.

(23) Wallington, T. J.; Hurley, M. D.; Shi, J.; Maricq, M. M.; Sehested, J.; Nielsen, O. J.; Ellermann, T. *Int. J. Chem. Kinet*. **1993**, *25*, 651.

(24) Collingwood, B.; Lee, H.; Wilmhurst, J. K. *Aust. J. Chem*. **1966**, *19*, 1637.

(25) Bellamy, L. J. *The Infra-red Spectra of Complex Molecules, Vols. 1 & 2*, 3rd Ed.; Chapman and Hall: London, 1975.

(26) Kaiser, E. W.; Wallington, T. J. *J. Phys. Chem*. **1995**, *99*, 8669.

(27) Mallard, W. G.; Westley, F.; Herron, J. T.; Hampson, R. F.; Frizzell, D. H. NIST Chemical Kinetics Database: Version 6.0, NIST, Gaithersburg, MD, 1994.

(28) Hassinen, E.; Riepponen, P.; Blomqvist, K.; Kalliorinne, K.; Evseev, A. M.; Koskikallio, J. *Int. J. Chem. Kinet.* **1985**, *17*, 1125.

(29) Japar, S. M.; Wallington, T. J.; Richert, J. F. O.; Ball, J. C. *Int. J. Chem. Kinet*. **1990**, *22*, 1257.

(30) Langer, S.; Ljungstrom, E.; Wängberg, I.; Wallington, T. J.; Hurley, M. D.; Nielsen, O. J. *Int. J. Chem. Kinet.* **1996**, *28*, 299.

(31) Wallington, T. J.; Hurley, M. D.; Ball, J. C.; Jenkin, M. E. *Chem. Phys. Lett*., **1993**, *211*, 41.

(32) Jenkin, M. E.; Hayman, G. D.; Wallington, T. J.; Hurley, M. D.; Ball, J. C.; Nielsen, O. J.; Ellermann, T. *J. Phys. Chem*. **1993**, *97*, 11712.

(33) Eberhard, J.; Müller, C.; Stocker, D. W.; Kerr, J. A. *Environ. Sci. Technol*. **1995**, *29*, 232.

(34) Atkinson, R.; Aschmann, S. M. *Int. J. Chem. Kinet*. **1995**, *27*, 261.

(35) Wallington, T. J.; Hurley, M. D.; Ball, J. C.; Platz, J.; Christensen, L. K.; Sehested; J.; Nielsen, O. J. *J. Phys. Chem*., submitted.

(36) Veyret, B.; Roussel, P.; Lesclaux, R. *Int. J. Chem. Kinet*. **1984**, *16*, 1599.

(37) Prinn, R.; Cunnold, D.; Simmonds, P.; Alyea, F.; Boldi, R.; Crawford, A.; Fraser, P.; Gutler, D.; Hartley, D.; Rosen, R.; Rasmussen, R. *J. Geophys. Res*. **1992**, *97*, 2445.

(38) Ravishankara, A. R.; Lovejoy, E. R. *J. Chem. Soc., Faraday Trans.* **1994**, *90*, 2159.

(39) Calvert, J. G.; Pitts, J. N, Jr. *Photochemistry*; John Wiley: New York, 1966.

(40) Atkinson, R. *Scientific Assessment of Stratospheric Ozone*, Report No. 20; World Meteorological Organization, Global Ozone Research and Monitoring Project: Geneva, Switzerland, 1989; Vol. 2, p 167.